nanomaterials

MDPI

Communication

Hydrophilic Modification of Gadolinium Oxide by Building Double Molecular Structures

Qin Li [1,†], Jian Chen [1,†], Xingwu Zhang [1], Chenjie Ruan [1] and Weiwei Wu [2,*]

[1] Yangjiang Nuclear Power Co., Ltd., Yangjiang 529941, China; 18506618870@163.com (Q.L.); chenjian_07@163.com (J.C.); zhangxingwu2025@163.com (X.Z.); powerjay03@163.com (C.R.)
[2] School of Information Mechanics and Sensing Engineering, Xidian University, Xi'an 710126, China
* Correspondence: wwwu@xidian.edu.cn
† These authors contributed equally to this work.

Abstract

With the rapid growth of nuclear energy, effective shielding of radioactive nuclear by-products is critical for safety and environmental protection. Gadolinium (Gd) is ideal for neutron shielding due to its exceptionally high thermal neutron capture cross-section. Despite significant progress in developing various Gd-based shielding materials, poor interfacial compatibility between Gd_2O_3 and polymer matrices remains a significant limitation. In this study, we addressed this challenge by successfully modifying Gd_2O_3 nanoparticles (Gd_2O_3@SIT-M) through the construction of a dual-layer molecular coating using electrostatic interactions. Initially, Gd_2O_3 was functionalized with the silane coupling agent 3-(trihydroxysilyl) propyl-1-propane-sulfonic acid (SIT), followed by subsequent assembly of polyether amine M2070 onto this modified surface. The combined presence of hydrophilic sulfonic acid groups from SIT and amine-ether groups from M2070 endowed Gd_2O_3@SIT-M nanoparticles with excellent hydrophilicity, significantly reducing their aqueous contact angle to 14.34°. Consequently, this modification strategy notably enhanced the dispersion stability of Gd_2O_3 nanoparticles in aqueous solutions and polymer matrices. The developed approach thus provides an effective pathway for fabricating advanced polymer-based neutron shielding materials with improved dispersibility, stability, and overall performance.

Keywords: Gd_2O_3 nanoparticle; surface modification; hydrophilic modification; polyether amine

check for updates

Academic Editor: Alessandro Barge

Received: 2 August 2025
Revised: 10 September 2025
Accepted: 12 September 2025
Published: 16 September 2025

Citation: Li, Q.; Chen, J.; Zhang, X.; Ruan, C.; Wu, W. Hydrophilic Modification of Gadolinium Oxide by Building Double Molecular Structures. *Nanomaterials* **2025**, *15*, 1421. https://doi.org/10.3390/nano15181421

Copyright: © 2025 by the authors. Licensee MDPI, Basel, Switzerland. This article is an open access article distributed under the terms and conditions of the Creative Commons Attribution (CC BY) license (https://creativecommons.org/licenses/by/4.0/).

1. Introduction

In recent decades, the extensive utilization of nuclear energy has significantly enhanced global energy supply, addressing the persistent challenge of balancing energy demands with environmental concerns. Currently, nuclear power provides approximately 10% of global electricity generation, substantially reducing greenhouse gas emissions compared to traditional fossil fuel-based sources [1,2]. As a sustainable and environmentally friendly alternative, nuclear energy thus occupies an increasingly vital position in modern energy strategies. Nevertheless, despite its notable benefits, the widespread application of nuclear energy is hindered by several critical issues, particularly the generation of radioactive byproducts during nuclear reactions. These byproducts emit various types of radiation, including alpha rays, beta rays, gamma rays, and neutrons [3–6]. Among these radiation types, neutron radiation has attracted significant attention due to its highly penetrating

nature and substantial capability to cause irradiation damage, presenting a major challenge in radiation shielding [4,7].

A promising strategy to enhance neutron shielding performance involves incorporating elements with large neutron capture cross-sections into protective materials. This approach significantly improves both the neutron absorption capacity and mechanical properties of shielding composites. The rare-earth element gadolinium (Gd), recognized for its exceptional neutron capture efficiency since its discovery by Dunning et al. in 1935 [8], has consistently been validated as highly effective for neutron shielding applications in subsequent research [9–11]. Specifically, the isotope ^{157}Gd possesses an extraordinarily high neutron capture cross-section of approximately 254,000 barns, which is about 67 times greater than the widely utilized neutron absorber, boron-10 (^{10}B), a commonly used neutron absorber with a cross-section of approximately 3800 barns [9,12]. Other materials, such as cadmium (Cd) with a cross-section of 2450 barns and samarium (Sm) with around 5900 barns for ^{149}Sm, also offer neutron absorption but fall short of Gd's efficiency [13]. Additionally, while boron-based compounds like B_4C are widely used, they are less effective against thermal neutrons compared to Gd_2O_3, and their incorporation into polymers often results in brittleness. Cadmium, although effective, poses environmental and health concerns due to its toxicity, making it less favorable for widespread use [14]. Moreover, Gd_2O_3 offers practical advantages over these alternatives. Unlike lead (Pb) or tungsten (W), which are effective against gamma and X-rays but poor neutron absorbers, Gd_2O_3 specifically targets neutron shielding. Consequently, gadolinium-based materials have been intensively explored as efficient neutron shielding candidates. Burke et al. [15], for instance, demonstrated that Gd_2O_3 coatings significantly improved radiation shielding performance through effective neutron attenuation and absorption.

Polymeric materials, including epoxy resin (ER), polyvinyl alcohol (PVA), and polyethylene (PE), have also emerged as attractive candidates for neutron shielding due to their capacity to moderate and scatter fast neutrons effectively [16]. However, their intrinsic thermal neutron shielding capabilities remain relatively limited. Thus, incorporating gadolinium compounds, particularly Gd_2O_3, into polymer matrices is a strategic approach to substantially enhance their neutron shielding effectiveness. Despite their potential, gadolinium-based polymer composites often encounter significant challenges related to poor interfacial compatibility between inorganic Gd_2O_3 fillers and organic polymer matrices, resulting in aggregation, poor dispersion stability, and diminished overall performance. For instance, Li et al. [17] revealed that nano-sized Gd_2O_3 particles demonstrated superior X-/γ-ray shielding performance compared to their micro-sized counterparts when incorporated into epoxy resins, attributable to their finer dispersion and smaller particle sizes. Nonetheless, the advantages of nanoscale particles diminished with increasing filler loading. Similarly, He et al. [18] reported that excessive nano-Gd_2O_3 incorporation adversely affected the thermal stability and mechanical properties of salicylic acid polyphenylene sulfide (SAPPS) composites. Furthermore, Huo et al. [19] indicated that surface-modified Gd_2O_3 particles significantly improved both thermal stability and mechanical properties in high-density polyethylene (HDPE) composites, demonstrating that surface modification is critical to addressing interfacial incompatibility and enhancing shielding performance.

Given the importance of effective interfacial interactions for achieving uniform dispersion and stable composite structures, this study aims to enhance the dispersibility and compatibility of Gd_2O_3 nanoparticles within aqueous and polymer matrices. Specifically, we introduced a two-step hydrophilic surface modification strategy involving an initial functionalization with organosilane SIT, followed by the assembly of a secondary layer through electrostatic interactions between negatively charged sulfonic acid groups from SIT and positively charged amino groups from polyether amine M2070. This bilayer

modification significantly improved the aqueous stability and dispersion uniformity of Gd_2O_3 nanoparticles, ultimately providing an efficient pathway toward high-performance polymer-based neutron shielding materials with optimized thermal, mechanical, and neutron attenuation properties.

2. Materials and Methods

Materials: 3-(trihydroxy silyl)propyl-1-propane-sulfonic acid (SIT, $C_3H_{10}O_6SSi$, 30–35% in water), Sodium hydroxide (NaOH, 98%), γ-aminopropyl triethoxysilane (KH-550, 99%) and γ-(2,3-epoxypropylene oxide) propyltrimethoxysilane (KH-560, 99%) was purchased from Macklin (Shanghai Macklin Biochemical Co., Ltd., Shanghai, China) and used as received. Type 732 strong acidic styrene cation-exchange resin with sulfonic acid groups was purchased from Aladdin (Shanghai Aladdin Bio-Chem Technology Co., Ltd., Shanghai, China). Polyetheramine (M2070, Mn∼2000, >98%) was bought from Suzhou Long Branch Industrial Co., Ltd. (Suzhou, China) Styrene cation exchange resin (Amberlite 732) was purchased from Aladdin (Melbourne, Australia). All other chemicals such as methanol and ethanol were of analytical grade and were used without further purification. Deionized water was used in the experiment.

Synthesis of Gd_2O_3@SIT: 0.5 g Gd_2O_3 nanoparticles (Gd_2O_3 NPs) were dispersed in 20 mL deionized water and ultrasound for 30 min to form a milky white Gd_2O_3 aqueous solution. Then, 1 g SIT was added to the DI water and then the pH was adjusted to 6–7 with 1 mol/L NaOH, which was mixed with the previous Gd_2O_3 aqueous solution and stirred for 12 h at room temperature. The product was dialyzed (a dialysis bag with 5000 molecular) for 12 h to remove the residual SIT during which the fresh DI water was altered every four hours. The suspension was added to the pre-treated 732 Styrene cation exchange resin with stirring at room temperature for 24 h to exchange the Na-type with the H-type. The obtained Gd_2O_3@SIT nanoparticles were filtered in DI water for future use.

Synthesis of Gd_2O_3@SIT-M: Gd_2O_3@SIT nanoparticles (0.5 g) were first dispersed in 20 mL aqueous solvent and sonicated for 10 min. Then, Polyether amine M2070 aqueous solution was drop-wise added to the above suspension until the pH reached 7 with constant stirring. The resulting solution was then dried on a hot plate fixed at 80 °C with stirring at 150 rpm/min and then kept at 50 °C under vacuum to obtain the Gd_2O_3@SIT-M sample.

Pretreatment process of cation exchange resin: The conditioning of the resin before the preconcentration procedure was conducted in order to remove any metal impurities. For this purpose, type 732 cation-exchange resin was successively washed with deionized water, 5% HCl solution, and deionized water.

Measurements: The attenuated total reflection infrared (ATR-IR) spectroscopy was conducted by a smart ATR-IR spectrometer (NicoletiS10, Thermo Fisher Scientific, Waltham, MA, USA) equipped with a smart OMNI reflection ranging from 400 to 4000 cm^{-1}. Zeta potentials of samples were analyzed by a zeta potential analyzer (Brookhaven Instruments, Nashua, USA). Contact angle measurements were performed using a contact angle goniometer (Theta Flex, Biolin, Finland). Thermo-gravimetric analysis (STA 449F5, Netzsch, Germany) experiments were carried out under a N_2 atmosphere with a heating rate of 5 °C/min. XRD patterns were recorded on an X-ray diffractometer (D8 ADVANCE, Bruker, Germany) focus advanced X-ray diffractometer operated at 40 kV and 40 mA using a Cu Ka radiation of wavelength (λ = 1.5406 Å). The equipment was calibrated by a standard silicon sample before measurement. Scanning electron microscopy (SEM) images were obtained from a field-emission scanning electron microscopy (FESEM, Apreo HiVac, FEI, Hillsboro, USA), at an accelerating voltage of 5 kV. Samples were dispersed in aqueous solution, attached on the conductive carbon adhesive tape, dried in a vacuum oven and then sputter-coated with 5 nm gold before observation. Transmission electron microscope

(TEM, JEM-2100F, JEOL, Tokyo, Japan) images were obtained by evaporating a drop of aqueous dispersion of samples on carbon-coated copper grids, followed by measurement on a Titan TEM operating at 120 kV.

3. Results

As illustrated in the schematic diagram of Figure 1, the hydrophilic modification of Gd_2O_3 nanoparticles is achieved via a two-step surface modification process. Initially, Gd_2O_3 particles are functionalized with the organosilane SIT, forming a stable intermediate layer through covalent bonding between the surface hydroxyl groups of Gd_2O_3 and silanol groups from SIT molecules. Subsequently, an additional polyether amine (M2070) layer is constructed onto the Gd_2O_3@SIT through electrostatic interactions between negatively charged sulfonic acid groups (–SO_3H) of SIT and positively charged amine groups of M2070, resulting in a robust double molecular layer.

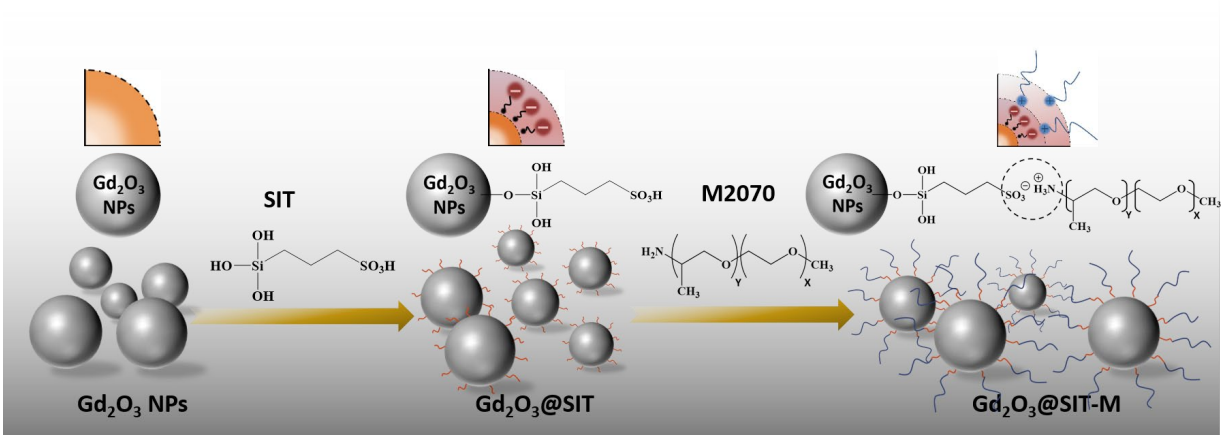

Figure 1. Schematic diagram of hydrophilic modification constructed by double molecular layer structure.

To systematically investigate the micromorphology evolution associated with each modification stage, pristine Gd_2O_3, Gd_2O_3@SIT, and Gd_2O_3@SIT-M samples were characterized by scanning electron microscopy (SEM) and transmission electron microscopy (TEM), as presented in Figure 2. As depicted in Figure 2a,b, pristine Gd_2O_3 particles exhibit clearly defined surfaces without the presence of any organic layers. In contrast, Figure 2c,d distinctly demonstrate the formation of a noticeable organic SIT layer covering the Gd_2O_3 surface after initial functionalization, significantly altering its surface texture and morphology. Furthermore, (Figure 2e,f) present SEM and TEM images of Gd_2O_3@SIT-M, revealing substantial lamellar structures and confirming an abundant and uniform distribution of the outer polyether amine layer (M2070). It is particularly noteworthy that the dual-layer organic modification plays a crucial role in enhancing the dispersibility and stability of Gd_2O_3 nanoparticles within aqueous solutions or polymer matrices. These improvements are anticipated to advance their applications as functional fillers for the development of novel neutron-shielding composite materials.

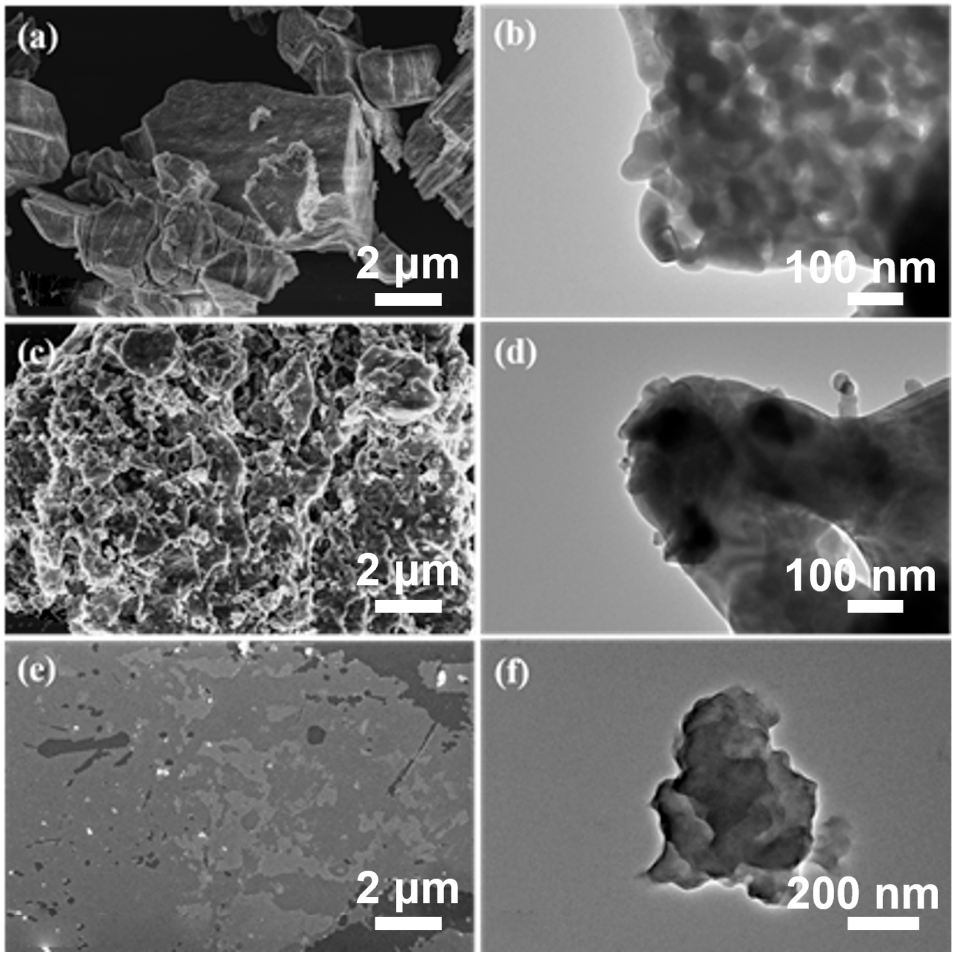

Figure 2. (**a**) SEM image and (**b**) TEM image of Gd_2O_3, (**c**) SEM image and (**d**) TEM image of Gd_2O_3@SIT, (**e**) SEM image and (**f**) TEM image of Gd_2O_3@SIT-M, respectively.

In the bright-field TEM image of Figure S1, the sample appears as an agglomerate of sub-micrometer primary particles with discernible interparticle boundaries. The corresponding EDS maps show that Gd and O are strongly co-localized across the entire particle body, confirming that the inorganic domains are Gd–O rich and consistent with Gd_2O_3. No segregated Gd-free or O-free regions are observed at the mapping resolution, indicating the absence of detectable secondary inorganic phases within the probed area. A weak but discernible Si signal is preferentially distributed along the outer rim of the agglomerate, suggesting a thin Si–O–containing surface layer at the particle periphery. This peripheral enrichment is consistent with the intended surface functionalization route that introduces Si-bearing moieties from SIT and does not alter the Gd–O-dominated core. The C map appears nearly uniform over the field of view; this is expected because it primarily originates from the supporting carbon film and, potentially, the organic surface ligands. Consequently, the C signal is not diagnostic of the inorganic core composition.

Subsequently, XRD analysis was performed on Gd_2O_3@SIT-M to elucidate its structural evolution. As presented in Figure 3, characteristic diffraction peaks observed at approximately 16.3°, 26.9°, and 28.9° can be attributed to the presence of $Gd(OH)_3$ phases [20]. To investigate the underlying cause of this physical phase transition, we also conducted comparative XRD analyses on samples modified individually with SIT, KH550, and KH560 (Figures S2–S4). These analyses produced nearly identical XRD patterns, indicating no detectable alteration in the crystal structure of Gd_2O_3 before ion-exchange treatment. However, after passing through the cation exchange resin, all modified samples uniformly exhibited a phase conversion to $Gd(OH)_3$. The detailed mechanisms responsible for this

phenomenon will be addressed comprehensively in our subsequent research. Additionally, upon the introduction of the polyether amine M2070, two new characteristic peaks emerged near 20°, as highlighted in Figure 3. These peaks likely originate from the formation of novel chelation complexes between M2070 and the functionalized surface of Gd_2O_3@SIT, a hypothesis that warrants further investigation.

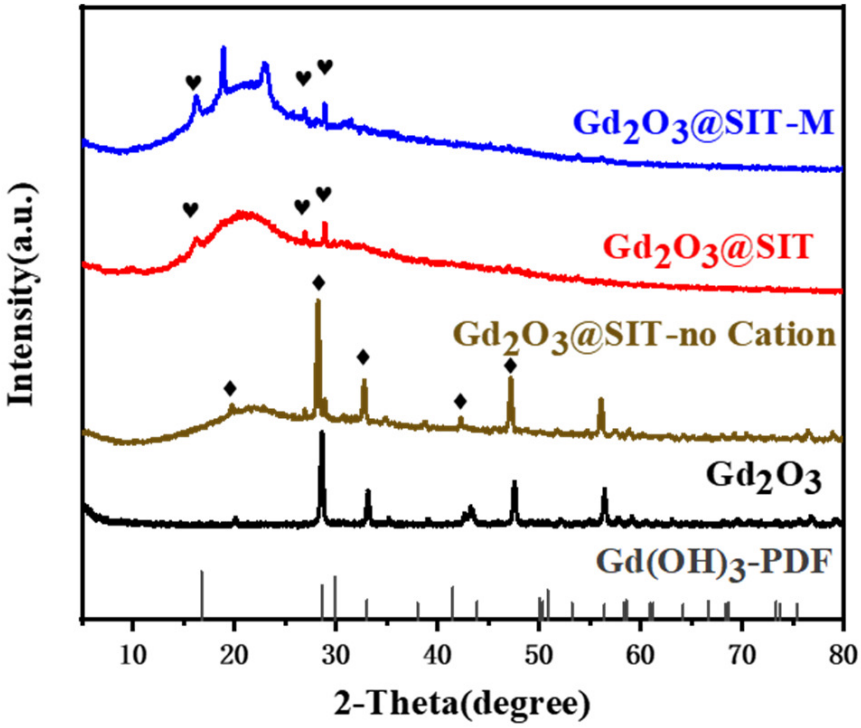

Figure 3. XRD patterns of Gd_2O_3, Gd_2O_3@SIT and Gd_2O_3@SIT-M. Heart symboles represent the dominant diffraction angles of $Gd(OH)_3$ and the diamond symboles represent the dominant diffraction angle of Gd_2O_3.

In addition, we further used the Rietveld refinement to calculate the lattice parameters. As shown in Figure S5 and Table S1, The crystallographic structures of the obtained samples were analyzed by Rietveld refinement of the powder X-ray diffraction (XRD) patterns, consistent with JCPDS card No. 86-2477 for Gd_2O_3 and JCPDS card No. 83-2037 for $Gd(OH)_3$ [20]. The quality of the refinement was evaluated by the profile residual (R_p), the weighted profile residual (R_{wp}), and the goodness-of-fit indicator (χ^2). The low values of R_p and R_{wp}, and χ^2 indicate a good agreement between the experimental and calculated diffraction patterns.

For sample 1 (Figure S5a), the diffraction peaks were sharp and intense, characteristic of a highly crystalline structure. The refined lattice parameters were a = b = c = 10.8099 Å, in good agreement with reported values for cubic system for Gd_2O_3. After acid treatment, the lattice parameters of the sample 2 exhibit noticeable changes, several characteristic reflections of Gd_2O_3 disappear or decrease in intensity, while new peaks emerge that can be assigned to hexagonal $Gd(OH)_3$. The refined lattice parameters of $Gd(OH)_3$ (a = b = 6.3291 Å, c = 3.6126 Å) are consistent with reported values, further validating the phase identification. The specific lattice parameters were summarized in Table S1.

Figure 4a presents the attenuated total reflection infrared (ATR-IR) spectra of pristine Gd_2O_3, Gd_2O_3@SIT, and Gd_2O_3@SIT-M samples. In the spectrum of Gd_2O_3@SIT-M, the prominent absorption band at approximately 544 cm^{-1} is attributed to the characteristic Gd–O vibrational modes of the inorganic core [15]. Additionally, the broad bands between 3500 and 2500 cm^{-1} correspond to the C–H stretching vibrations originating from the

polymer backbone of the polyether amine (M2070) [21]. Distinct absorption peaks observed at 1311 cm^{-1} and 1168 cm^{-1} can be assigned to the symmetric and asymmetric stretching vibrations of sulfonate groups (O=S=O), respectively, confirming the successful modification by SIT molecules [22]. Furthermore, the intense peak at approximately 1060 cm^{-1} is characteristic of the asymmetric stretching vibration mode of Si–O–Si bonds from the SIT layer. The strong, broad band observed around 3470 cm^{-1} indicates the presence of O–H stretching and bending vibrations, which can likely be attributed to hydroxyl groups formed as a result of the cation exchange resin treatment, causing partial conversion of Gd_2O_3 to $Gd(OH)_3$ [23].

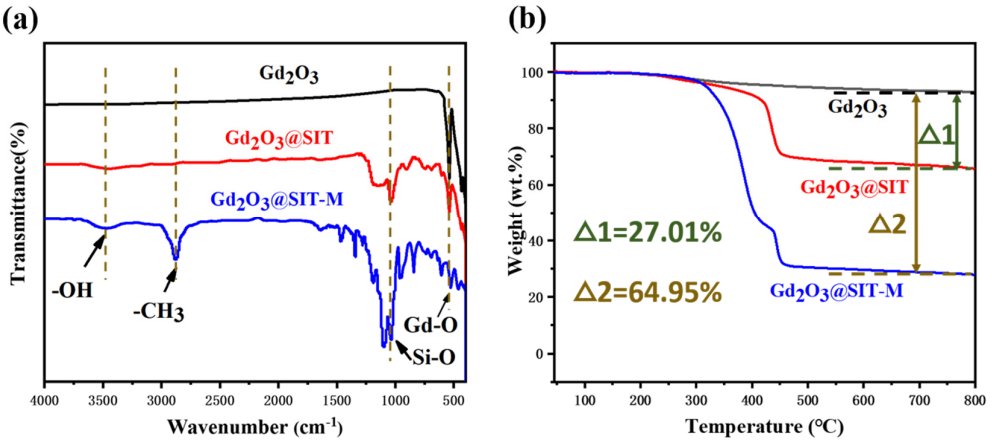

Figure 4. (**a**) ATR-IR spectroscopy of Gd_2O_3, Gd_2O_3@SIT and Gd_2O_3@SIT-M, (**b**) TGA traces of Gd_2O_3, Gd_2O_3@SIT and Gd_2O_3@SIT-M under N_2 atmosphere at 5 °C/min.

Figure 4b displays the thermogravimetric analysis (TGA) curves for pristine Gd_2O_3, Gd_2O_3@SIT, and Gd_2O_3@SIT-M under a nitrogen atmosphere with a heating rate of 5 °C/min. It is notable that neither Gd_2O_3@SIT nor Gd_2O_3@SIT-M exhibited any discernible weight loss below 200 °C, indicating the absence of residual aqueous solvents and confirming their negligible volatility. As the temperature increased beyond 250 °C, decomposition of the organic molecular layers began, with Gd_2O_3@SIT-M displaying a higher decomposition rate compared to Gd_2O_3@SIT. This accelerated decomposition can be attributed to the comparatively weaker thermal stability of the polyether amine (M2070) polymer chains. A plateau occurring around 430 °C in the TGA curve of Gd_2O_3@SIT-M reflects the distinct thermolysis temperatures of the bilayer organic structure, implying stepwise decomposition of the SIT and M2070 layers. Upon further increasing the temperature to 800 °C, the residual weight percentages of Gd_2O_3@SIT and Gd_2O_3@SIT-M were determined as 66.01 wt.% and 28.06 wt.%, respectively. This indicates that the dual molecular organic layers in Gd_2O_3@SIT-M constituted approximately 64.95 wt.% of the total mass, thereby significantly enhancing its hydrophilic character and dispersibility.

As illustrated in Figure 5a, the measured contact angles of pristine Gd_2O_3 and modified Gd_2O_3@SIT-M were 74.10° and 14.34°, respectively. This significant reduction in the contact angle indicates a marked enhancement in the hydrophilicity of Gd_2O_3, attributable to the successful construction of a bilayer organic coating on its surface. To quantitatively assess the stability of these particles in aqueous media, zeta potential measurements were performed. As depicted in Figure 5b, the zeta potential of Gd_2O_3@SIT-M (−28.2 mV) is substantially lower compared to that of pristine Gd_2O_3 (−12.36 mV). This enhanced negative surface charge arises from the introduction of the hydrophilic organic layers, which effectively increases surface wettability and electrostatic repulsion among particles, thus improving their aqueous dispersibility and stability.

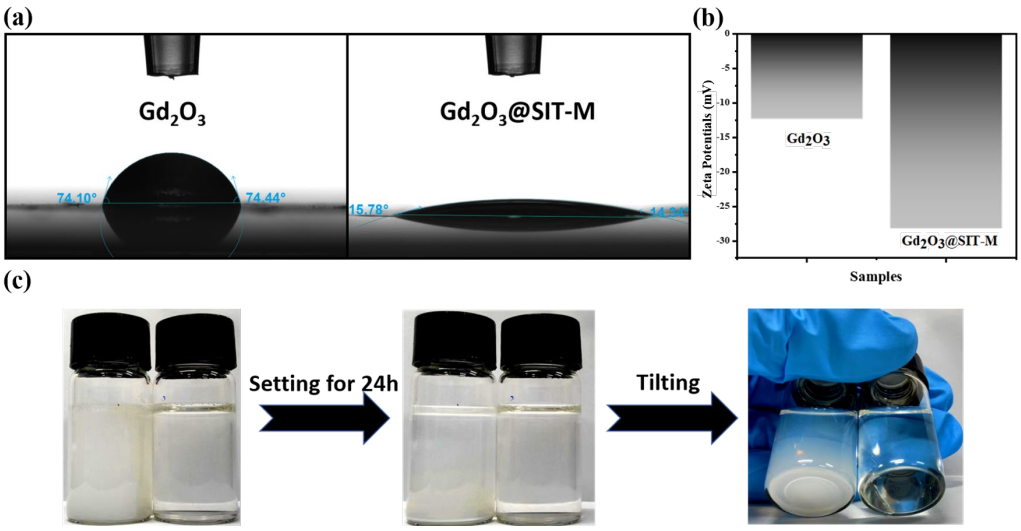

Figure 5. (**a**) Contact angles of Gd_2O_3 and Gd_2O_3@SIT-M, (**b**) Zeta potentials of Gd_2O_3 and Gd_2O_3@SIT-M in aqueous solution, (**c**) Photographs of aqueous stabilities of 10.0 mg/mL of Gd_2O_3 (left) and Gd_2O_3@SIT-M (right).

To further confirm dispersion stability, aqueous dispersions with a concentration of 10.0 mg/mL for both pristine Gd_2O_3 and Gd_2O_3@SIT-M were prepared and allowed to stand undisturbed at room temperature for 24 h. As shown in Figure 5c, visible sedimentation occurred in the pristine Gd_2O_3 suspension, while no precipitation or agglomeration was observed in the Gd_2O_3@SIT-M dispersion, even upon tilting. This clearly demonstrates that the modified Gd_2O_3@SIT-M possesses superior colloidal stability in aqueous environments compared to unmodified Gd_2O_3. Furthermore, as shown in Supplementary Figure S6, after storage at room temperature for three months, Gd_2O_3@SIT-M remained dispersible and stable in an aqueous medium for at least 24 h without observable sedimentation. Collectively, these results conclusively illustrate that the electrostatically assembled hydrophilic double-layer structure formed on the Gd_2O_3 surface effectively prevents particle aggregation and sedimentation, resulting in stable and uniformly dispersed aqueous suspensions suitable for long-term practical applications.

4. Conclusions

In summary, hydrophilically modified Gd_2O_3 nanoparticles coated with double organic molecular layers were successfully fabricated through a two-step modification process involving the organosilane SIT and the polyether amine M2070. The initial modification step involved covalent bonding between hydroxyl groups on the Gd_2O_3 surface and the silanol groups of SIT, creating an intermediate surface layer with negatively charged sulfonic acid groups. Subsequently, electrostatic interactions between these negatively charged sulfonic acid groups on Gd_2O_3@SIT and positively charged amino groups on M2070 facilitated the formation of a stable and robust bilayer structure, referred to as Gd_2O_3@SIT-M. Characterization results confirmed that the hydrophilic bilayer modification significantly enhanced the dispersion stability of Gd_2O_3 nanoparticles in aqueous solutions. The remarkable improvement in dispersibility is primarily attributed to the presence of hydrophilic polar groups—namely, sulfonic acid groups in SIT and amine groups in M2070—on the nanoparticle surfaces, which effectively promote interactions with water molecules. Moreover, the introduction of these bilayers substantially reduced the water contact angle and lowered the zeta potential, further indicating enhanced hydrophilicity and colloidal stability. Thermogravimetric analysis (TGA) verified the presence and thermal stability of the dual organic coating, highlighting its robustness at moderate temperatures.

Consequently, the modified Gd_2O_3@SIT-M nanoparticles exhibit excellent aqueous dispersion stability, remaining uniformly dispersed without aggregation or sedimentation even after extended periods of storage. Such outstanding dispersibility in aqueous and polymer matrices positions these materials as promising candidates for incorporation into functional composites, especially in neutron shielding applications. This novel surface modification strategy not only ensures improved material compatibility but also provides a solid foundation for developing advanced neutron-shielding materials with enhanced processability and performance.

Supplementary Materials: The following supporting information can be downloaded at: https://www.mdpi.com/article/10.3390/nano15181421/s1, Figure S1: The EDS mapping of Gd_2O_3@SIT containing the elements of C, O, Si, and Gd; Figure S2: XRD patterns of Gd_2O_3, Gd_2O_3@SIT and Gd_2O_3@SIT-no Cation; Figure S3: XRD patterns of Gd_2O_3, Gd_2O_3@KH550 and Gd2O3@KH550-no Cation; Figure S4: XRD patterns of Gd_2O_3, Gd_2O_3@KH560 and Gd_2O_3@KH560-no Cation; Figure S5: Rietveld refinement of the XRD patterns for the synthesized samples; Figure S6: Photographs of aqueous stabilities of 10.0 mg/mL of long-standing Gd_2O_3@SIT-M. Table S1: The lattice parameters of the Sample 1 (Gd_2O_3) and Sample 2 ($Gd(OH)_3$ and Gd_2O_3) according to the XRD refinement analysis.

Author Contributions: Conceptualization, W.W. and Q.L.; methodology and investigation, Q.L. and J.C.; data curation, Q.L., J.C., X.Z., and C.R.; writing—original draft preparation, Q.L. and J.C.; writing—review and editing, W.W., Q.L., J.C., X.Z., and C.R.; supervision, W.W.; funding acquisition, W.W. All authors have read and agreed to the published version of the manuscript.

Funding: The authors thank the financial support from Research and Development Project on New Multifunctional Lightweight Neutron and Gamma-Ray Composite Shielding Materials for Yangjiang Nuclear Power Plant (NO. N-KY-HX-1117-202309-06245).

Data Availability Statement: Dataset available from the corresponding author upon request.

Conflicts of Interest: Qin Li, Jian Chen, Xingwu Zhang and Chenjie Ruan were employed by the company Yangjiang Nuclear Power Co., Ltd. The remaining author declares that the research was conducted in the absence of any commercial or financial relationships that could be construed as a potential conflict of interest.

References

1. Peters, I.M. Strategic global deployment of photovoltaic technology: Balancing economic capacity and decarbonization potential. *Adv. Atmos. Sci.* **2025**, *42*, 261–268. [CrossRef]
2. Wang, J.; Chen, X.; Zhuang, M.; Li, Y.; Ruan, Z.; Wang, Y.; Zhang, N.; Song, J.; He, K.; Lu, X. Accelerating exploitation and integration of global renewable energy. *Innovation* **2025**, *6*, 100873. [CrossRef]
3. Ewing, R.C. Long-term storage of spent nuclear fuel. *Nat. Mater.* **2015**, *14*, 252–257. [CrossRef]
4. Kursun, C.; Gao, M.; Yalcin, A.O.; Parrey, K.A.; Gaylan, Y. Structure, mechanical, and neutron radiation shielding characteristics of mechanically milled nanostructured (100-x) Al-xGd_2O_3 metal composites. *Ceram. Int.* **2024**, *50*, 27154–27164. [CrossRef]
5. Tyagi, G.; Singhal, A.; Routroy, S.; Bhunia, D.; Lahoti, M. Radiation Shielding Concrete with alternate constituents: An approach to address multiple hazards. *J. Hazard. Mater.* **2021**, *404*, 124201. [CrossRef]
6. Mishra, G.; Bhadouria, V.S.; Ray, D.; Chauhan, S.; Saraswat, S.P.; Dixit, S.; Sawood, G.M. Radioactive Waste: A Catastrophic Waste. In *Global Waste Management*; Scrivener Publishing LLC: Beverly, MA, USA, 2025; pp. 145–193.
7. Chen, Y.; Lin, Q.; Zhu, W.; Tang, M.; Li, H.; Li, G.; Fan, Z. A scientometric review of knowledge domains on nuclear radiation. *J. Radiat. Res. Appl. Sci.* **2024**, *17*, 100995. [CrossRef]
8. Dunning, J.; Pegram, G.; Fink, G.; Mitchell, D. Interaction of neutrons with matter. *Phys. Rev.* **1935**, *48*, 265. [CrossRef]
9. Wang, K.; Ma, L.; Yang, C.; Bian, Z.; Zhang, D.; Cui, S.; Wang, M.; Chen, Z.; Li, X. Recent progress in Gd-containing materials for neutron shielding applications: A review. *Materials* **2023**, *16*, 4305. [CrossRef]
10. Jopat, P.R.; Paul, S.; Sen, S.; Bahadur, J.; Patra, G.D.; Samanta, S.; Pathak, A.; Kulkarni, M.S. $LiAlO_2$: Gd-based versatile and ultrasensitive detector for gamma and neutrons by thermal and optical stimulation. *ACS Appl. Mater. Interfaces* **2024**, *16*, 39642–39655. [CrossRef]
11. Zhang, C.; Shi, Y.; Wang, X.; Qi, J.; Lu, T. Mechanical, photoluminescent properties and energy transfer mechanism of highly transparent $(Y_{0.99-x}Gd_xSm_{0.01})_2O_3$ ceramics for scintillator applications. *J. Eur. Ceram. Soc.* **2024**, *44*, 1783–1794. [CrossRef]

12. Ho, S.L.; Yue, H.; Tegafaw, T.; Ahmad, M.Y.; Liu, S.; Nam, S.-W.; Chang, Y.; Lee, G.H. Gadolinium neutron capture therapy (GdNCT) agents from molecular to nano: Current status and perspectives. *ACS Omega* **2022**, *7*, 2533–2553. [CrossRef]
13. Hidaka, H. Isotopic variations of Sm, Gd, Er and Yb found in planetary materials caused by neutron-capture reactions in nature. *J. Anal. Sci. Technol.* **2024**, *15*, 14. [CrossRef]
14. Ramadan, B.S.; Wibowo, Y.G.; Anwar, D.; Maryani, A.T. A review of life cycle assessment of nanomaterials-based adsorbent for environmental remediation. *Glob. NEST J.* **2024**, *26*, 6216. [CrossRef]
15. Burke, D.; Byun, S. Feasibility of gadolinium oxide paint as neutron shielding. *Nucl. Instrum. Methods Phys. Res. Sect. A* **2022**, *1025*, 166175. [CrossRef]
16. Prabhu, S.; Bubbly, S.; Gudennavar, S.B. X-ray and γ-ray shielding efficiency of polymer composites: Choice of fillers, effect of loading and filler size, photon energy and multifunctionality. *Polym. Rev.* **2023**, *63*, 246–288. [CrossRef]
17. Li, R.; Gu, Y.; Wang, Y.; Yang, Z.; Li, M.; Zhang, Z. Effect of particle size on gamma radiation shielding property of gadolinium oxide dispersed epoxy resin matrix composite. *Mater. Res. Express* **2017**, *4*, 035035. [CrossRef]
18. He, Y.; Li, P.; Ren, H.; Zhang, X.; Chen, X.; Yan, Y. The fabrication and neutron shielding property of polyphenylene sulfide containing salicylic acid/Gd_2O_3 composites. *High Perform. Polym.* **2022**, *34*, 105–114. [CrossRef]
19. Huo, Z.; Zhao, S.; Zhong, G.; Zhang, H.; Hu, L. Surface modified-gadolinium/boron/polyethylene composite with high shielding performance for neutron and gamma-ray. *Nucl. Mater. Energy* **2021**, *29*, 101095. [CrossRef]
20. Chen, F.; Zhang, X.H.; Hu, X.D.; Zhang, W.; Zeng, R.; Liu, P.D.; Zhang, H.Q. Synthesis and characteristics of nanorods of gadolinium hydroxide and gadolinium oxide. *J. Alloys Compd.* **2016**, *664*, 311–316. [CrossRef]
21. Balomenou, G.; Stathi, P.; Enotiadis, A.; Gournis, D.; Deligiannakis, Y. Physicochemical study of amino-functionalized organosilicon cubes intercalated in montmorillonite clay: H-binding and metal uptake. *J. Colloid Interface Sci.* **2008**, *325*, 74–83. [CrossRef]
22. Zhang, W.; Zhang, B.; He, G.; Liu, B.; Jiang, Z.; Yang, X.; Li, C. Enhanced water retention and proton conductivity of proton exchange membranes by incorporating hollow polymer microspheres grafted with sulfonated polystyrene brushes. *RSC Adv.* **2015**, *5*, 5343–5356. [CrossRef]
23. Tajdini, B.; Vatankhah, H.; Pezoulas, E.R.; Zhang, C.; Higgins, C.P.; Bellona, C. Adsorbability of a wide range of per-and polyfluoroalkyl substances on granular activated carbon, ion exchange resin, and surface modified clay. *Water Res.* **2025**, *268*, 122774.

Disclaimer/Publisher's Note: The statements, opinions and data contained in all publications are solely those of the individual author(s) and contributor(s) and not of MDPI and/or the editor(s). MDPI and/or the editor(s) disclaim responsibility for any injury to people or property resulting from any ideas, methods, instructions or products referred to in the content.